J Mater Sci (2015) 50:6469–6476
DOI 10.1007/s10853-015-9205-8

A laminar nanocomposite constructed by self-assembly of exfoliated α-ZrP nanosheets and manganese porphyrin for use in the electrocatalytic oxidation of nitrite

Binbin Pan[1] · Juanjuan Ma[2] · Xiaobo Zhang[2] · Jinpeng Li[2] · Lin Liu[2] · Dongen Zhang[2] · Min Yang[2] · Zhiwei Tong[1,2,3]

Received: 23 April 2015 / Accepted: 23 June 2015 / Published online: 2 July 2015

Abstract Laminar nanocomposite of α-ZrP/MnTMPyP, [5, 10, 15, 20-tetrakis (*N*-methylpyridinium-4-yl) porphyrinato manganese (III)], was obtained through the self-assembly of α-ZrP nanosheets and manganese porphyrin molecules, namely the exfoliation/restacking route. The final products were characterized by several analytic techniques such as XRD, IR, UV–Vis, and SEM. Meanwhile, the surface charge change of layered zirconium phosphate during the restacking process was monitored by a Zetasizer Nano instrument. The zeta potential value of α-ZrP colloidal dispersion is −40.1 mV, indicating that the colloidal dispersion was stable and well dispersed. The cyclic voltammetry measurements of α-ZrP/MnTMPyP film-modified glass carbon electrode displayed a pair of well-defined oxidation/reduction peaks with redox potentials at −0.256 and −0.197 V with an increase in the peak current compared to MnTMPyP aqueous solution. Furthermore, α-ZrP/MnTMPyP hybrid thin film exhibited excellent electrocatalytic activities toward oxidation of nitrite. The oxidation peak current increased linearly with the square root of scan rate, suggesting that the electrocatalytic process was controlled by nitrite diffusion. Finally, a detection limit of 5.3×10^{-5} M was estimated at a signal-to-noise ratio of 3.0 with a concentration range of 1.5×10^{-4} to 4.76×10^{-3} M.

Introduction

In recent years, two-dimension layered materials have drawn considerable interest in numerous fields including photochemistry, electrochemistry, and catalysis mainly due to their particular structure and characteristics [1–5]. As a kind of artificial layered materials firstly discovered by

Electronic supplementary material The online version of this article (doi:10.1007/s10853-015-9205-8) contains supplementary material, which is available to authorized users.

✉ Zhiwei Tong
zhiweitong575@hotmail.com

Binbin Pan
pbb1015125196@126.com

Juanjuan Ma
majj0518@hotmail.com

Xiaobo Zhang
zhxiaobo@163.com

Jinpeng Li
1209325202@qq.com

Lin Liu
spliulin@fzu.edu.cn

Dongen Zhang
zdewxm@aliyun.com

Min Yang
1097487702@qq.com

[1] School of Chemical Engineering and Technology, China University of Mining and Technology, Xuzhou 221116, China

[2] School of Chemical Engineering, Huaihai Institute of Technology, Lianyungang 222005, China

[3] SORST, Japan Science and Technology Agency (JST), Kawaguchi Center Building 4-1-8, Kawaguchi-shi, Saitama 332-0012, Japan

Clearfield and Stynes in 1964 [6], α-$Zr(HPO_4)_2·H_2O$ (abbreviated as α-ZrP) owns several characteristics such as larger surface charge density and higher aspect ratio and ion-exchange capacity [7–10] except for commonalities of layered nanomaterials. Hence, some related articles about preparation of the intercalation compounds of α-ZrP/MB (methylene blue) [11], α-ZrP/porphyrin [12], α-ZrP/hemoglobin [13–15], and α-ZrP/insulin [16] were reported. In addition, α-ZrP has been modified to obtain various hybrid materials with diverse applications by replacing hydroxyl groups located on the surface of α-ZrP with organic functional groups [17, 18]. Concerning the structure of α-ZrP, three oxygen atoms belonging to one phosphate group are bonded to three different Zr atoms forming the laminate, while OH connecting to P atoms points into the interlayer region or on the surface [19] (Fig. 1).

As a well-known class of compounds extensively existed in biological systems, porphyrins and their derivatives play an important role in several aspects of oxygen transfer (Hemoglobin), storage (Myohemoglobin), activation (Cytochrome), and photosynthesis (Chlorophyll). The multifunctional composites constructed by the immobilization of porphyrin derivatives in various inorganic layered materials have become the research focus [20–24].

Many efforts have been devoted to the preparation of nanocomposites through the ion-exchange process previously which usually takes a longer period [25–27]. Nevertheless, time-saving exfoliation/restacking route has attracted considerable interests recently due to opening access to explore the inner surface of laminate. At present, much attention was paid to delamination of transition metal dichalcogenides (MoS_2) [28], layered double hydroxides (LDHs) [29–32], and metal oxides ($Ca_2Nb_3O_{10}^-$, $TiNbO_5^-$) [33–35]; meanwhile, the exfoliation of α-ZrP nanosheets has also become the research focus [36–39]. Therefore, it is promising to introduce metalloporphyrin into the interlayer of α-ZrP through the exfoliation/restacking method (Fig. 2).

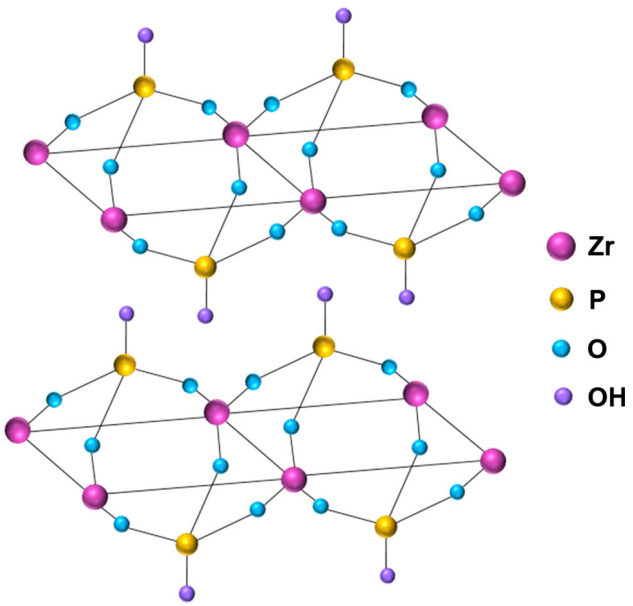

Fig. 1 Schematic structure of α-$Zr(HPO_4)_2·H_2O$

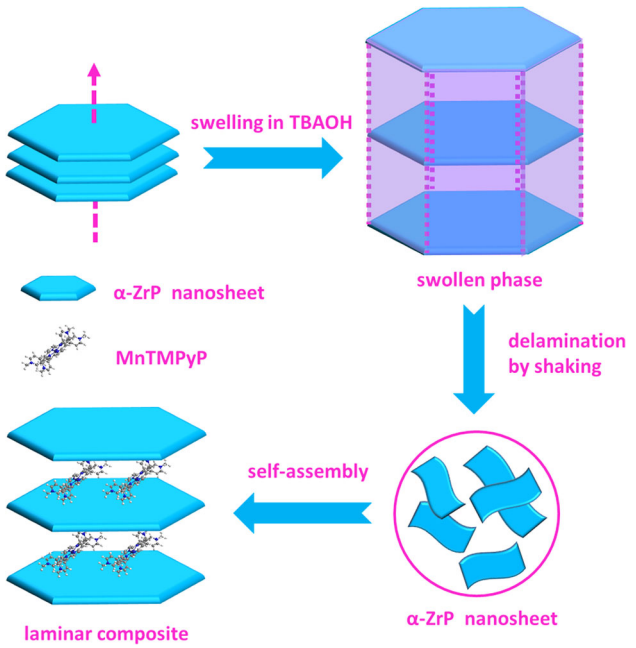

Fig. 2 Schematic illustration of the reassembly process between α-ZrP nanosheets and metalloporphyrin

As a kind of common inorganic pollutant in environment and food industry, nitrite can be converted to N-nitrous compounds which are carcinogenic to humans. The quantitative analysis of nitrite can be achieved by electrochemical method [40]. Herein, we made an attempt to fabricate α-ZrP/MnTMPyP lamellar nanocomposite via electrostatic interaction between manganese porphyrin aqueous solution and colloidal dispersion of α-ZrP nanosheets, so that we could make further research on electrochemical determination of nitrite.

Experimental

Preparation of exfoliated α-ZrP nanosheets

α-ZrP was prepared by a slightly modified HF approach reported in previous literature [41]. 3.0 g $ZrOCl_2·8H_2O$ powder dispersed in 30 ml distilled water beforehand was mixed with 9 ml phosphoric acid and 3 ml hydrofluoric acid at 80 °C in a plastic flask, and the resulting white precipitate was collected by centrifugation, washed with distilled water several times, and dried at 50 °C. Typically, 0.05 g α-ZrP material was then dispersed into thirty milliliters distilled water with stoichiometric amounts of

10 (wt%) TBAOH aqueous solution and agitated uniformly for 3 days in a single-necked flask; the resulting translucent colloidal suspension was centrifuged at 6000 rpm to remove the unexfoliated particles to avoid affecting the later experiments.

Fabrication of α-ZrP/MnTMPyP intercalation hybrids

Regarding the fabrication of α-ZrP/MnTMPyP intercalation hybrids, 1 mM MnTMPyP aqueous solution was added into the colloidal dispersion of α-ZrP mentioned above. The precipitate was centrifuged under 8000 rpm, washed with distilled water several times, and dried at 50 °C for further characterization.

Characterization

X-ray diffraction patterns were collected with a RINT 2000 diffractometer (Rigaku) using Cu Kα radiation ($\lambda = 0.154$ nm) with 2θ from 2° to 40°. Zeta potential of α-ZrP colloidal suspension was monitored using a Malvern Zetasizer Nano instrument, and water at 25 °C was selected as the dispersion solvent. Infrared spectra were measured on a Shimadzu FTIR-8400S spectrometer with the use of KBr pellets. UV–Vis absorption spectra were recorded on a UV–vis spectrometer (UV-2550). The morphology of the samples was investigated by a scanning electron microscopic apparatus (JEOL, JSM-6390), and the specimens should be treated by spray-gold firstly.

Electrochemical characterization and property

The electrochemical experiments were carried out in a conventional three-electrode cell at room temperature, with a platinum wire electrode as the counter electrode, a saturated calomel electrode (SCE) as the reference electrode, and the α-ZrP/MnTMPyP hybrid thin film-modified glass carbon electrode (GCE) as the working electrode. The acting electrolyte was 0.2 mol L^{-1} phosphate buffer solution (PBS) which should be purged with N_2 for 20 min before examination to avoid the influence of oxygen. Cyclic voltammetry (CV) and differential pulse voltammetry (DPV) scans were all carried out on a CHI660c electrochemical workstation.

Results and discussion

XRD analysis

Figure 3 shows the XRD patterns of α-ZrP host material and α-ZrP/MnTMPyP intercalation compound. It can be clearly seen that α-ZrP sample with high crystallinity exhibited intense diffraction peaks, and the interlayer distance was calculated as 0.75 nm according to 2θ angle (11.75°) of the 002 characteristic peak, while the interlayer distance of the restacking product increases to 1.64 nm with the lower 2θ angle of 5.4°. With respect to the fabrication of α-ZrP colloidal dispersion and MnTMPyP aqueous solution, it should be attributed to the electrostatic interaction between the negatively charged α-ZrP nanosheets and metalloporphyrin cations with ESD mechanism [42]. In order to investigate the angle of MnTMPyP located in the galley of the hybrid, the rough calculation was made as follows. Considering the host layer thickness of 0.63 nm [38], a conclusion can be drawn that MnTMPyP molecules were placed into the interlayer by a monolayer inclined angle of 34° according to the known size of MnTMPyP ring (18.0 × 18.0 × 7.5 Å, estimated by MM2 method).

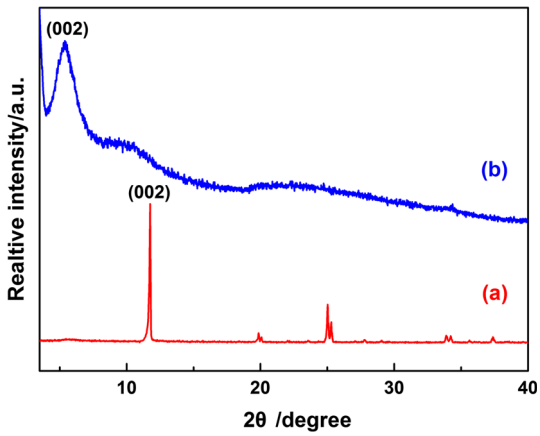

Fig. 3 XRD patterns of **a** α-ZrP host material and **b** α-ZrP/MnTMPyP hybrid

Zeta potential analysis

To further confirm the restacking process, the detection of the surface potential was achieved by a Zetasizer Nano instrument. The zeta potential of α-ZrP colloidal dispersion is −40.1 mV, which indicated that the dispersion was stable and well dispersed. In order to acquire zero potential point of reaction, a few volume ratios of α-ZrP colloidal dispersion and MnTMPyP aqueous solution were tested as shown in Fig. S1; the zeta potential increases with the addition of MnTMPyP aqueous solution, and it turned out that the zeta potential of the 1:0.58 ratio approaches nearly zero. Flocculation phenomenon about coassembly of α-ZrP nanosheets and MnTMPyP aqueous solution at this ratio was displayed in Fig. 4b, and the reaction is extremely fast and can be finished within 20 min which is superior to the traditional ion-exchange method. As observed in Fig. 4a, clear Tyndall light scattering was found in the colloidal

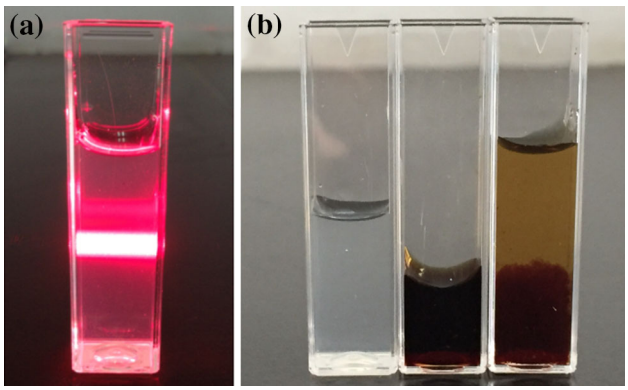

Fig. 4 **a** Tyndall phenomenon of colloidal dispersion of exfoliated α-ZrP nanosheets, **b** photographs of colloidal suspensions of α-ZrP nanosheets in TBAOH aqueous solution (*left*), MnTMPyP aqueous solution (*middle*), and the corresponding mixture of α-ZrP and MnTMPyP (*right*)

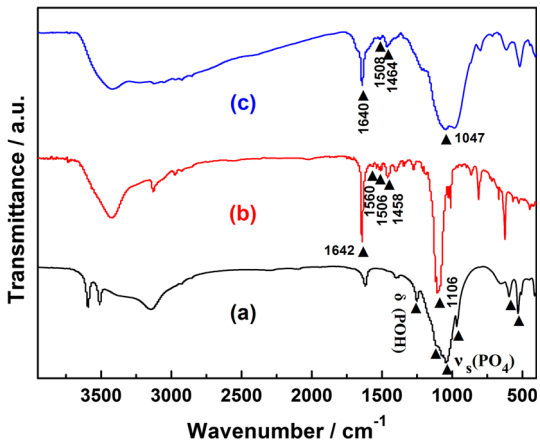

Fig. 5 FT-IR spectra of *a* α-ZrP, *b* MnTMPyP, and *c* α-ZrP/MnTMPyP

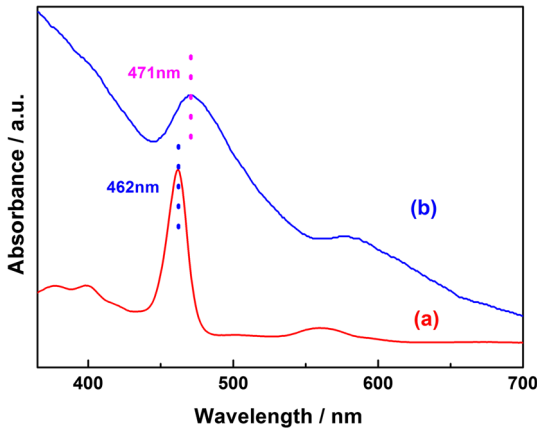

Fig. 6 UV–visible absorption spectra of *a* MnTMPyP aqueous solution and *b* α-ZrP/MnTMPyP hybrid film

solution of α-ZrP nanosheets, suggesting the occurrence of exfoliation [29].

IR spectra analysis

The characteristic peaks of MnTMPyP at 1642, 1560, 1506, and 1458 cm^{-1} correspond to stretching vibration of C=N or C=C in the pyridine substituent and porphyrin rings (Fig. 5). Besides, the absorption bands at 1106 cm^{-1} should be assigned to the single bond of C–N. The infrared spectrum of α-ZrP/MnTMPyP hybrid exhibited similar absorption in the range of 1700–1000 cm^{-1} with a slight shift merely, possibly attributing to interaction of intercalated guest molecules and the host layer [43]. As noted by line (a), these bands ascribed to the phosphate groups [36] in the host layer were also present in IR spectrum of α-ZrP/MnTMPyP intercalation compound.

UV–Visible absorption spectra analysis

Figure 6 gives UV–Vis spectra of MnTMPyP aqueous solution and α-ZrP/MnTMPyP nanocomposite. Compared with MnTMPyP aqueous solution, the hybrid exhibits a 9-nm red shift in the Soret band caused by restricted manganese porphyrin molecules located in the galley consistent with several analogous reports [44, 45]. The existence of a broadening phenomenon in the hybrid was due to some degree of aggregation and stacking of the metalloporphyrin molecules [46].

SEM analysis

As observed in Fig. 7, the origin material of α-ZrP with high crystallinity reveals a large average size of about 1–3 μm. While, the introduction of MnTMPyP led to the formation of intercalation hybrid with irregular shape and rough surface. However, two-dimensional layered structure of the final composite was reconstructed by the reassembly of α-ZrP nanosheets and MnTMPyP molecules.

Electrochemical characterization

The CV curves of MnTMPyP aqueous solution and α-ZrP/MnTMPyP hybrid film in pH 7.0 PBS at 50 mV s^{-1} scan rate are shown in Fig. 8. A couple of well-defined oxidation/reduction peaks with redox potentials were at −0.257 and −0.183 V for MnTMPyP aqueous solution, with the midpoint potential $E_m = (E_{pa} + E_{pc})/2 = -0.22$ V and the peak separation $\Delta E_p = 74$ mV. A couple of similar electrochemical characteristic oxidation/reduction peaks appear in α-ZrP/MnTMPyP hybrid film-modified GCE at −0.256 and −0.197 V, respectively, and the peak separation ΔE_p was reduced to 59 mV.

As shown in Fig. 9, the CV experiments of the modified electrode in 0.2 M PBS at different scan rates from 50 to

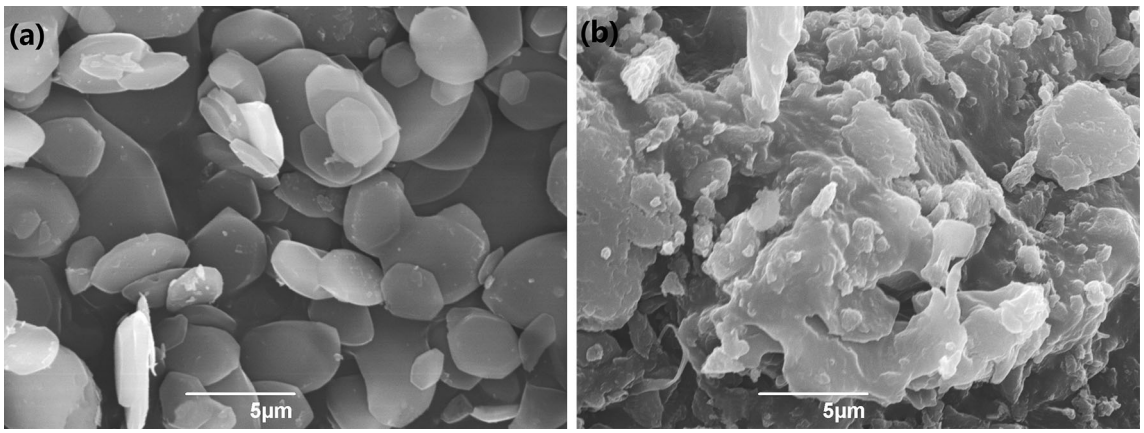

Fig. 7 SEM images of **a** α-ZrP and **b** α-ZrP/MnTMPyP

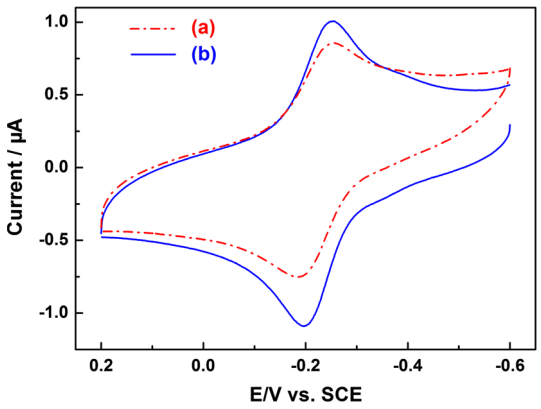

Fig. 8 CV curves of *a* MnTMPyP aqueous solution (*dash line*) and *b* α-ZrP/MnTMPyP-modified GCE (*solid line*) in N_2-saturated pH 7.0 PBS solution at 50 mV s^{-1}

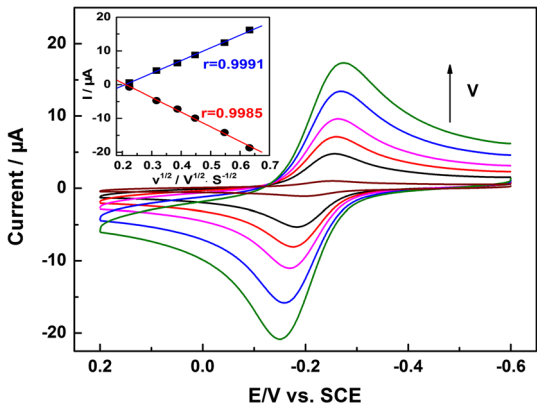

Fig. 9 CV curves of α-ZrP/MnTMPyP-modified GCE in N_2-saturated pH 7.0 PBS solution at 50, 100, 150, 200, 300, and 400 mV s^{-1}; the inset is the relationship curve between I and $v^{1/2}$

400 mV s^{-1} were conducted. It is observed that the anodic peak shifted positively and the cathodic peak shifted negatively with the increase of the scan rate. Meanwhile, the peak separation ΔE_p went from 59 mV to 123 mV as well owing to the steric hindrance effect of the host layer [47]. The linear relationship of peak current (I) and square root of the scan rate ($v^{1/2}$) was expressed in the attached drawing. The calibration equations are I_{pa} (μA) = 9.19 − 43.32 $v^{1/2}$ ($V^{1/2}$ $s^{-1/2}$) ($r = 0.9985$) and I_{pc} (μA) = −7.87 + 37.57 $v^{1/2}$ ($V^{1/2}$ $s^{-1/2}$) ($r = 0.9991$).

Electrocatalytic activities of α-ZrP/MnTMPyP hybrid film toward oxidation of nitrite

As can be seen from Fig. 10, α-ZrP/MnTMPyP hybrid film-modified GCE shows good electrocatalytic activities toward oxidation of nitrite in pH 7.0 PBS. The oxidation peak potential at 0.997 V should be assigned to bare GCE, which is corresponding to the conversion of NO_2^- to NO_3^- through a two-electron oxidation process, while the oxidation peak potential of the modified electrode shifts

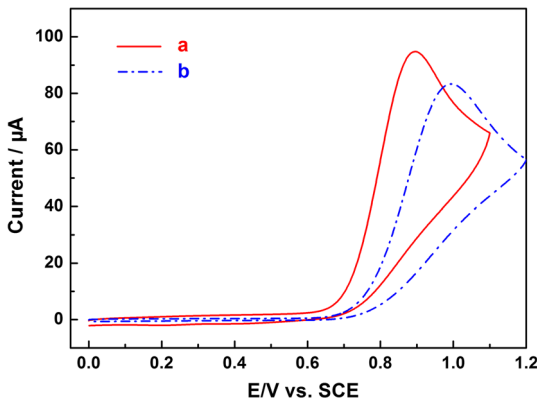

Fig. 10 CV curves of *a* α-ZrP/MnTMPyP-modified GCE (*solid line*) and *b* bare GCE (*dash line*) in N_2-saturated pH 7.0 PBS solution containing 4 mM $NaNO_2$ at 100 mV s^{-1}

negatively toward 0.897 V with an increase in peak current at a certain degree indicating that α-ZrP/MnTMPyP nanocomposite can efficiently promote the oxidation of NO_2^- [42].

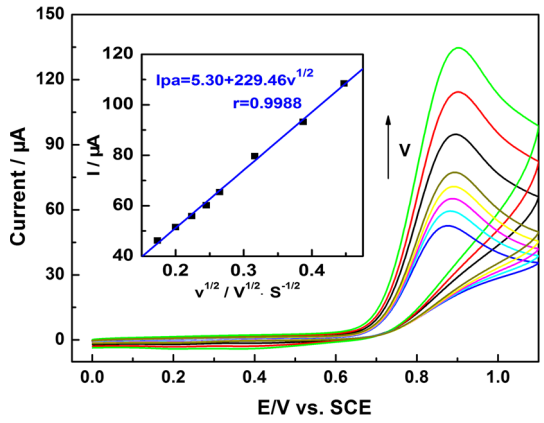

Fig. 11 CV curves of α-ZrP/MnTMPyP-modified GCE in N_2-saturated pH 7.0 PBS solution containing 4 mM $NaNO_2$ at 30, 40, 50, 60, 70, 100, 150, and 200 mV s^{-1}; the *inset* is the relationship curve between I_{pa} and $v^{1/2}$

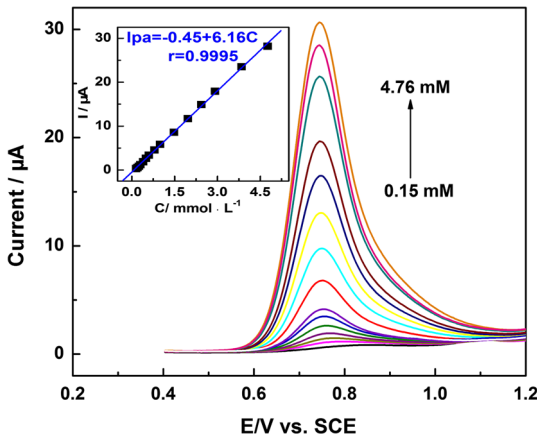

Fig. 12 DPV curves of α-ZrP/MnTMPyP-modified GCE in N_2-saturated pH 7.0 PBS solution with the $NaNO_2$ concentration ranging from 0.15 to 4.76 mM; the *inset* is the relationship curve between I_{pa} and c

According to related literatures [48], the mechanism of electrocatalytic oxidation on nitrite of the modified electrode can be illustrated using the following equations:

$$Mn^{III}TMPyP^{5+} + NO_2^- \rightleftharpoons \left[Mn^{II}TMPyP\ (NO_2)\right]^{4+} \quad (1)$$

$$\left[Mn^{II}TMPyP\ (NO_2)\right]^{4+} \rightleftharpoons Mn^{III}TMPyP^{5+} + NO_2 + e^- \quad (2)$$

$$2NO_2 + H_2O \rightleftharpoons 2H^+ + NO_3^- + NO_2^- \quad (3)$$

$$NO_2^- + H_2O \rightarrow 2H^+ + NO_3^- + 2e^- \quad (4)$$

With the purpose of investigating the influence of the scan rate toward peak current, the CV curves of the modified electrode at different scan rates from 30 to 200 mV s^{-1} were made. It can be seen that the anodic peak potential shifts positively with the increase of scan rate observed in Fig. 11. The inset shows linear relationship between peak current (I_{pa}) and square root of the scan rate ($v^{1/2}$), in the light of the calibration equation: I (μA) = 5.30 + 229.46 $v^{1/2}$ ($V^{1/2}$ $s^{-1/2}$) (r = 0.9988), electrochemical oxidation of nitrite on the surface of the modified electrode should be defined as an irreversible diffusion-controlled process [49].

In order to realize the quantitative analysis of the modified electrode toward nitrite oxidation, differential pulse voltammetry experiments were conducted with the NO_2^- concentration ranging from 0.15 to 4.76 mM shown in Fig. 12. The linear relationship between the peak current (I_{pa}) and the concentration of nitrite was observed in the inset whose calibration equation can be expressed as I (μA) = −0.45 + 6.16c (mmol L^{-1}) (r = 0.9995). According to a signal-to-noise ratio of 3.0, the detection limit of 5.3 × 10^{-5} M was estimated.

Conclusions

A convenient method called the exfoliation/restacking route was adopted to prepare α-ZrP/MnTMPyP laminar nanocomposite. The α-ZrP colloidal suspension obtained in the delamination process was traced by a Zetasizer Nano instrument. In addition, the arrangement of MnTMPyP molecule in the galley of the hybrid has been proposed. The CV measurements of α-ZrP/MnTMPyP film-modified GCE indicated that the as-obtained nanocomposite has exhibited excellent electrocatalytic activities on the oxidation of nitrite in pH 7.0 PBS. A detection limit of 5.3 × 10^{-5} M was estimated at a signal-to-noise ratio of 3.0 indicated by DPV results.

Acknowledgements This work was supported by National Natural Science Foundation of China (Grant Nos. 21401062, 21201070), Natural Science Fund of Jiangsu Province (BK20140447, BK20141247, SBK201220654), and University Science Research Project of Jiangsu Province (13KJB430005, 12KJD150001).

References

1. Tong Z et al (2006) Photoresponsive multilayer spiral nanotubes: intercalation of polyfluorinated cationic azobenzene surfactant into potassium niobate. J Am Chem Soc 128:684–685
2. Hosogi Y, Kato H, Kudo A (2008) Photocatalytic activities of layered titanates and niobates ion-exchanged with Sn^{2+} under visible light irradiation. J Phys Chem C 112:17678–17682
3. Zhang X et al (2010) Intercalation of methylene blue into layered potassium titanoniobate $KTiNbO_5$: characterization and electrochemical investigation. J Mater Sci 45:1604–1609. doi:10.1007/s10853-009-4134-z

4. Han J et al (2011) Layer-by-layer assembly of layered double hydroxide/cobalt phthalocyanine ultrathin film and its application for sensors. J Mater Chem 21:2126–2130
5. Ma J et al (2014) Facile assembly for fast construction of intercalation hybrids of layered double hydroxides with anionic metalloporphyrin. Dalton Trans 43:9909–9915
6. Clearfield A, Stynes JA (1964) The preparation of crystalline zirconium phosphate and some observations on its ion exchange behaviour. J Inorg Nucl Chem 26:117–129
7. Clearfield A (1984) Inorganic ion exchangers with layered structures. Ann Rev Mater Sci 14:205–229
8. Alberti G et al (1996) Layered and pillared metal (IV) phosphates and phosphonates. Adv Mater 8:291–303
9. Sun L et al (2005) Effect of crystallinity on the intercalation of monoamine in α-zirconium phosphate layer structure. Chem Mater 17:5606–5609
10. Xiao H et al (2015) Amine-intercalated α-zirconium phosphates as lubricant additives. Appl Surf Sci 329:384–389
11. Wang H et al (2005) Study on the intercalation and interlayer state of porphyrins into α-zirconium phosphate. J Incl Phenom Macro 52:247–252
12. Dilgin Y et al (2005) Photoelectrochemical investigation of methylene blue immobilised on zirconium phosphate modified carbon paste electrode in flow injection system. Anal Chim Acta 542:162–168
13. Liu Y et al (2008) Direct electron transfer of hemoglobin in layered α-zirconium phosphate with a high thermal stability. Anal Biochem 375:27–34
14. Kumar CV, Chaudhari A (2002) High temperature peroxidase activities of HRP and hemoglobin in the galleries of layered Zr (IV) phosphate. Chem Commun 20:2382–2383
15. Bhambhani A, Kumar CV (2006) Tuning the properties of Hb intercalated in the galleries of α-ZrP with ionic strength: improved structure retention and enhanced activity. Chem Mater 18:740–747
16. Díaz A et al (2010) Nanoencapsulation of insulin into zirconium phosphate for oral delivery applications. Biomacromolecules 11:2465–2470
17. Mosby BM et al (2013) Surface functionalization of zirconium phosphate nanoplatelets for the design of polymer fillers. ACS Appl Mater Interfaces 6:585–592
18. Mosby BM et al (2014) Designable architectures on nanoparticle surfaces: zirconium phosphate nanoplatelets as a platform for tetravalent metal and phosphonic acid assemblies. Langmuir 30:2513–2521
19. Troup JM, Clearfield A (1977) Mechanism of ion exchange in zirconium phosphates. 20. Refinement of the crystal structure of alpha-zirconium phosphate. Inorg Chem 16:3311–3314
20. Dias PM, De Faria DLA, Constantino VRL (2000) Spectroscopic studies on the interaction of tetramethylpyridylporphyrins and cationic clays. J Incl Phenom Macro 38:251–266
21. Bizeto MA, De Faria DLA, Constantino VRL (2002) Porphyrin intercalation into a layered niobate derived from $K_4Nb_6O_{17}$. J Mater Sci 37:265–270. doi:10.1023/A:1013687825874
22. Tong Z, Shichi T, Takagi K (2002) Visible-light induced charge-separation between consecutively cast porphyrin and methyl viologen multilayered titanoniobate hybrid films. J Phys Chem B 106:13306–13310
23. Kameyama H et al (2006) Oxidation of cyclohexene with molecular oxygen catalyzed by cobalt porphyrin complexes immobilized on montmorillonite. J Mol Catal A-chem 258:172–177
24. Kaschak DM et al (1999) Photoinduced energy and electron transfer reactions in lamellar polyanion/polycation thin films: toward an inorganic "leaf". J Am Chem Soc 121:3435–3445
25. Zhang X et al (2009) Preparation and electrochemical behavior of methylene blue intercalated into layered niobate $K_4Nb_6O_{17}$. J Mater Sci 44:3020–3025. doi:10.1007/s10853-009-3398-7
26. Shao F et al (2013) Synthesis and electrochemical properties study of novel intercalation compound of $KCa_2Nb_3O_{10}$ with cationic methylene blue. Micro Nano Lett 8:788–791
27. Guo X et al (2005) Synthesis of a novel super-microporous layered material and its catalytic application in the vapor-phase Beckmann rearrangement of cyclohexanone oxime. Micropor Mesopor Mat 80:269–274
28. Coleman JN et al (2011) Two-dimensional nanosheets produced by liquid exfoliation of layered materials. Science 331:568–571
29. Liu Z et al (2006) Synthesis, anion exchange, and delamination of Co-Al layered double hydroxide: assembly of the exfoliated nanosheet/polyanion composite films and magneto-optical studies. J Am Chem Soc 128:4872–4880
30. Liu Z et al (2007) General synthesis and delamination of highly crystalline transition-metal-bearing layered double hydroxides. Langmuir 23:861–867
31. Wang Y et al (2014) Coassembly of exfoliated Ni–In LDHs nanosheets with DNA and infrared emissivity study. J Mater Sci 49:6944–6951. doi:10.1007/s10853-014-8399-5
32. Yu J et al (2015) One-step direct synthesis of layered double hydroxide single-layer nanosheets. Nanoscale 7:9448–9451
33. Oshima T et al (2015) Intercalation of highly dispersed metal nanoclusters into a layered metal oxide for photocatalytic overall water splitting. Angew Chem Int Edit 54:2698–2702
34. Zhai Z et al (2012) Novel mesoporous NiO/$HTiNbO_5$ nanohybrids with high visible-light photocatalytic activity and good biocompatibility. Nanoscale 4:547–556
35. Zhang L et al (2013) S-doped $HTiNbO_5$ nanosheets: a novel efficient visible-light photocatalyst. Chin J Catal 34:2089–2097
36. Takei T et al (2006) Anodic electrodeposition of highly oriented zirconium phosphate and polyaniline-intercalated zirconium phosphate films. J Am Chem Soc 128:16634–16640
37. Kaschak DM et al (1998) Chemistry on the edge: a microscopic analysis of the intercalation, exfoliation, edge functionalization, and monolayer surface tiling reactions of α-zirconium phosphate. J Am Chem Soc 120:10887–10894
38. Kim HN et al (1997) Characterization of zirconium phosphate/polycation thin films grown by sequential adsorption reactions. Chem Mater 9:1414–1421
39. Sun L et al (2007) Preparation of exfoliated epoxy/α-zirconium phosphate nanocomposites containing high aspect ratio nanoplatelets. Chem Mater 19:1749–1754
40. Zhang X et al (2014) A manganese porphyrin intercalated lanthanum niobic acid nanocomposite utilized for electrocatalytic oxidation of nitrite. ECS Electrochem Lett 3:H17–H19
41. Alberti G, Torracca E (1968) Crystalline insoluble salts of polybasic metals-II. Synthesis of crystalline zirconium or titanium phosphate by direct precipitation. J Inorg Nucl Chem 30:317–318
42. Ma J et al (2015) Sandwich-structured composite from the direct coassembly of layered titanate nanosheets and Mn porphyrin and its electrocatalytic performance for nitrite oxidation. Mater Lett 150:122–125
43. Park IY, Kuroda K, Kato C (1989) Preparation of a layered double hydroxide-porphyrin intercalation compound. Chem Lett 11:2057–2058
44. Barloy L et al (1992) Manganese porphyrins adsorbed or intercalated in different mineral matrices: preparation and compared properties as catalysts for alkene and alkane oxidation. Mater Sci Forum 91:838

45. Halma M et al (2009) Immobilization of anionic iron (III) porphyrins into ordered macroporous layered double hydroxides and investigation of catalytic activity in oxidation reactions. J Mol Catal A 310:42–50
46. Halma M et al (2008) Synthesis, characterization, and catalytic activity of anionic iron (III) porphyrins intercalated into layered double hydroxides. J Catal 257:233–243
47. Zhang X et al (2013) Electrochemical investigation of a novel metalloporphyrin intercalated layered niobate modified electrode and its electrocatalysis on ascorbic acid. J Solid State Electr 17:3177–3184
48. Armijo F et al (2007) Electrocatalytic oxidation of nitrite to nitrate mediated by Fe(III) poly-3-aminophenyl porphyrin grown on five different electrode surface. J Mol Catal A 268:148–154
49. Zuo G et al (2007) Study of orientation mode of cobalt-porphyrin on the surface of gold electrode by electrocatalytic dioxygen reduction. J Mol Catal A 269:46–52